IJAME
Int. J. of Applied Mechanics and Engineering, 2026, vol.31, No.1, pp.16-26
DOI: 10.59441/ijame/213219

FRACTIONAL NATURAL CONVECTION HEAT TRANSFER ANALYSIS OF GO-MOS$_2$ ENGINE OIL WITHIN AN OSCILLATING VERTICAL CYLINDER

I. Elkott[1*], M.S. Abdel Latif [1,2], I.L. El-Kalla[1] and A.H. Abdel Kader[1,2]
[1]Department of Mathematics and Engineering Physics, Engineering Faculty, Mansoura University, Mansoura, EGYPT
[2]Department of Mathematics, Faculty of Science, New Mansoura University, New Mansoura City, EGYPT
E-mail: ebrahim.abd_elmonem@mans.edu.eg

In this study, we demonstrate the application of Laplace and finite Hankel transforms to obtain closed form solutions for the temperature and velocity profiles of a system governed by fractional differential equations. These equations model heat transfer through natural convection of a particular engine oil (EO) containing molybdenum disulphide and graphene oxide (MoS_2 + GO) hybrid nano-composites within an oscillating vertical cylinder (OVC). Several figures are presented to depict the influence of the Prandtl number and the fractional derivative order on the temperature profile and the Nusselt number.

Key words: fractional derivative, heat transfer, integral transforms, differential equations.

1. Introduction

The process of heat exchange among bodies through the movement of fluid currents is referred to as convective heat transfer [1]. Numerous studies have investigated energy transfer resulting from convection in cylindrical geometries, as demonstrated in previous works [2-5]. EO is utilized as a lubricant inside engines of various types of machinery [6-9]. Also, EO minimizes friction and wear of the engine's internal moving parts. By forming a thin layer of pressurized lubricant that fills the tiny gaps between various engine components, it prevents rough metal-to-metal contact. Furthermore, EO also helps regulate the engine's temperature by dissipating the heat generated during combustion. Another vital function of oil is to keep the engine clean by removing accumulated dirt and debris. This keeps corrosion at bay and improves the fuel efficiency of the machines, ensuring optimal performance. The natural convection heat transfer (NCHT) of an incompressible viscous EO in an OVC can be represented by [10]:

$$\theta_t(r,t)=\frac{1}{Pr}\left(\theta_{rr}(r,t)+\frac{1}{r}\theta_r(r,t)\right),\quad 0<r\langle 1,t\rangle 0 \tag{1.1}$$

$$u_t(r,t)=u_{rr}(r,t)+\frac{1}{r}u_r(r,t)+Gr\,\theta(r,t), \tag{1.2}$$

with the initial and boundary conditions

$$\theta(r,0)=0,\quad \theta(1,t)=1,\quad u(r,0)=0,\quad u_t(r,0)=0,\quad u(1,t)=H(t)\exp(i\omega t), \tag{1.3}$$

[*] To whom correspondence should be addressed

In reference [11], the researchers employed EO as the base fluid and incorporated molybdenum disulphide (MoS_2 + GO) hybrid nano-composites into the EO. Their findings indicated that the Maxwell hybrid nanofluid (GO + MoS_2 + EO) improved the heat transfer rate by as much as *23.17%*.
Consequently, the NCHT of GO-MoS_2 EO within an OVC can be represented by the following model

$$\theta_t(r,t)=\frac{b_2}{Pr}\left(\theta_{rr}(r,t)+\frac{1}{r}\theta_r(r,t)\right), \tag{1.4}$$

$$b_0u_t(r,t)+b_0\lambda u_{tt}(r,t)=u_{rr}(r,t)+\frac{1}{r}u_r(r,t)+b_1Gr\,\theta(r,t)+b_1Gr\,\lambda\theta_t(r,t), \tag{1.5}$$

with the initial conditions (1.3). Here, λ is the Maxwell fluid parameter, whereas b_0, b_1 and b_2 are coefficients that depend on the properties of the EO.
Fractional calculus, along with its applications across numerous scientific and engineering disciplines, is presently considered a vital area of mathematics [12-22]. The exploration and advancement of fractional partial differential equations (FPDEs) have garnered heightened attention, as these equations can more precisely represent a range of physical and chemical phenomena compared to conventional integer-order differential equations [12-15].In this paper, we investigate the NCHT of GO-MoS_2 EO within an OVC, which is modeled using the aforementioned FPDEs

$${}_0^cD_t^{\alpha}\theta=\frac{b_2}{Pr}\left(\theta_{rr}+\frac{1}{r}\theta_r\right),\quad 0<\alpha<1, \tag{1.6}$$

$$b_0\,{}_0^cD_t^{\gamma}u+b_0\lambda\,{}_0^cD_t^{\beta}u=u_{rr}+\frac{1}{r}u_r+b_1Gr\,\theta+b_1Gr\lambda\,{}_0^cD_t^{\alpha}\theta,\quad 0<\gamma<1,\quad 1<\beta<2, \tag{1.7}$$

with the conditions (1.3), where ${}_0^cD_t^{\rho}\theta$, is the fractional derivative of Caputo type of θ with respect to t defined by [16]

$${}_0^cD_t^{\rho}f(t)=\frac{1}{\Gamma(m-\rho)}\int_a^t(t-u)^{m-\rho-1}f^{[m]}(u)\,du,\quad m-1<\rho<m. \tag{1.8}$$

Integral transforms such as Laplace, Fourier, Hankel, Finite Fourier and Finite Hankel have been successfully used for about two centuries in solving numerous problems in engineering science, applied mathematics, and mathematical physics. The integral transform technique enables us to remove partial derivatives from the considered equations to obtain an algebraic equation in the transformed domain. Therefore, Laplace and finite Hankel transforms will be utilized for solving Eq.(1.6) and Eq.(1.7). This is how the remainder of the paper is structured:
Section 2 provides examples of certain fundamental fractional calculus definitions and theorems.
Sections 3 and 4, respectively, examine the solutions to Eq.(1.6) and Eq.(1.7).

2. Fundamental definitions

Definition 1 [22]. The Mittag-Leffler function (MLF) with one parameter $E_{\alpha}(z)$ is defined as

$$E_a(x)=\sum_{k=0}^{\infty}\frac{x^k}{\Gamma(ak+1)}\,. \tag{2.1}$$

Also, the two parameters MLF $E_{\alpha,\beta}(z)$ is given by

$$E_{a,b}(x)=\sum_{k=0}^{\infty}\frac{x^k}{\Gamma(ak+b)}, \tag{2.2}$$

and the three parameters MLF $E^{\gamma}_{\alpha,\beta}(z)$ is defined as

$$E^{\delta}_{a,b}(x)=\sum_{k=0}^{\infty}\frac{x^k\,\Gamma(\delta+k)}{\Gamma(ak+b)\Gamma(\delta)k!}. \tag{2.3}$$

Definition 2 [23]. For $0\le r\le a$, the finite Hankel transform of order zero (FHT) of $f(r)$ is

$$\mathcal{H}_0\{f(r)\}=\tilde{f}_0(r_n)=\int_0^a r\,J_0(r\,r_n)\,f(r)\,dr, \tag{2.4}$$

$J_0(z)$ represents the Bessel function of the first kind of order zero, while r_n denote zeros of $J_0(a\,r_n)=0$.

Definition 3 [23]. For $0\le r\le a$, the inverse FHT of $\tilde{f}_0(r_n)$ can be formulated as

$$\mathcal{H}_0^{-1}\{\tilde{f}_0(r_n)\}=f(r)=\frac{2}{a^2}\sum_{n=1}^{\infty}\tilde{f}_0(r_n)\frac{J_0(r\,r_n)}{J_1^2(a\,r_n)}. \tag{2.5}$$

Definition 4 [24]. The lower incomplete gamma function $\Upsilon(s\,,x)$ can be represented by

$$\Upsilon(s\,,x)=x^s\,\Gamma(s)e^{-x}\sum_{k=0}^{\infty}\frac{x^k}{\Gamma(s+k+1)}=x^s\,\Gamma(s)e^{-x}E_{1,s+1}(x). \tag{2.6}$$

Lemma 1 [23]. The FHT of $\left\{\frac{1}{r}\frac{d}{dr}\left(r\frac{df(r)}{dr}\right)\right\}$ is given by

$$\mathcal{H}_0\left\{\frac{1}{r}\frac{d}{dr}\left(r\frac{df(r)}{dr}\right)\right\}=-r_n^{\,2}\,\tilde{f}_0(r_n)+a\,r_n\,f(a)J_1(a\,r_n). \tag{2.7}$$

Lemma 2 [22]. The Laplace transform (LT) of the Caputo derivative (2.8) is

$$L\left\{{}_0^cD_t^{\rho}f(t)\right\}=s^{\rho}L\{f(t)\}-s^{\rho-1}f(0)+s^{\rho-2}f'(0),\quad 0<\rho<2. \tag{2.8}$$

$$L\left\{{}_0^cD_t^{\rho}f(t)\right\}=s^{\rho}L\{f(t)\}-s^{\rho-1}f(0),\quad 0<\rho<1. \tag{2.9}$$

Lemma 3 [22].

$$1.\ L^{-1}\left\{\frac{1}{a s^{\alpha_1}+b s^{\alpha_2}+1}\right\}=\sum_{k=0}^{\infty}\frac{(-b)^k}{(a)^{k+1}}t^{(1+k)\alpha_1-k\alpha_2-1}E^{k+1}_{\alpha_1,(1+k)\alpha_1-k\alpha_2}\left(\frac{-1}{a}t^{\alpha_1}\right),\quad \alpha_1>\alpha_2, \tag{2.10}$$

$$2.\ L^{-1}\left\{\frac{a}{s(s^{\alpha}+a)}\right\}=1-E_{\alpha}\left(-a t^{\alpha}\right), \tag{2.11}$$

$$3.\ L^{-1}\left\{\frac{1}{s^{1-\alpha}(s^{\alpha}+a)}\right\}=E_{\alpha}\left(-a t^{\alpha}\right). \tag{2.12}$$

Lemma 4 [25-26]. The integrations of two functions are illustrated

$$1.\ \int_0^t \tau^{\beta}\, e^{x(t-\tau)}\mathrm{d}\tau = e^{xt}\, x^{-1-\beta}\ \Upsilon\left(\beta+1,\, xt\right), \tag{2.13}$$

$$2.\ \int_0^t \tau^{\beta} E_{\alpha}\left(-a(t-\tau)^{\alpha}\right)du = \Gamma(\beta+1)(t)^{\beta+1}\ E_{\alpha,\beta+2}\left(-a t^{\alpha}\right). \tag{2.14}$$

3. Exact solution for the temperature of the fluid

Applying the FHT (2.4) to Eq.(1.6) and utilizing Eq.(2.7), we get

$${}_0^c D_t^{\alpha}\theta(r_n,t)=\frac{b_2}{Pr}\left(-r_n^2\theta(r_n,t)+r_n J_1(r_n)\theta(1,t)\right). \tag{3.1}$$

Since $\theta(1,t)=1,$ we get

$${}_0^c D_t^{\alpha}\theta(r_n,t)=\frac{b_2}{Pr}\left(-r_n^2\,\theta(r_n,t)+r_n J_1(r_n)\right). \tag{3.2}$$

Apply the LT to Eq.(3.1), to get

$$s^{\alpha}L\left[\theta(r_n,t)\right]-s^{\alpha-1}\theta(r_n,0)=\frac{-b_2}{Pr}r_n^2\,L\left[\theta(r_n,t)\right]+\frac{b_2}{Pr}r_n J_1(r_n)\frac{1}{s}. \tag{3.3}$$

Since $\theta(r_n,0)=0,$ we get

$$s^{\alpha}L\left[\theta(r_n,t)\right]=\frac{-b_2}{Pr}r_n^2\,L\left[\theta(r_n,t)\right]+\frac{b_2}{\mathrm{p_r}}r_n J_1(r_n)\frac{1}{s}. \tag{3.4}$$

Solving Eq.(3.4) for $L\left[\theta(r_n,t)\right]$, we obtain

$$L\left[\theta(r_n,t)\right]=\frac{\frac{b_2 r_n^2}{Pr}}{s\left(s^{\alpha}+\frac{b_2 r_n^2}{Pr}\right)}\frac{J_1(r_n)}{r_n}. \tag{3.5}$$

Applying inverse LT to Eq.(3.5) and utilizing Eq.(2.11), we get

$$\theta(r_n,t)=\frac{J_1(r_n)}{r_n}\left(1-E_{\alpha}\left(-\frac{b_2 r_n^2}{Pr}t^{\alpha}\right)\right). \tag{3.6}$$

By applying the inverse FHT Eq.(2.5) to Eq.(3.6), we get

$$\begin{aligned}\theta(r,t)&=2\sum_{n=1}^{\infty}\frac{J_0(r\,r_n)}{J_1^2(r_n)}\frac{J_1(r_n)}{r_n}\left(1-E_{\alpha}\left(-\frac{b_2 r_n^2}{Pr}t^{\alpha}\right)\right)=\\&=2\sum_{n=1}^{\infty}\frac{J_0(r\,r_n)}{J_1^2(r_n)}\frac{J_1(r_n)}{r_n}-2\sum_{n=1}^{\infty}\frac{J_0(rr_n)}{J_1^2(r_n)}\frac{J_1(r_n)}{r_n}E_{\alpha}\left(-\frac{b_2 r_n^2}{Pr}t^{\alpha}\right)=\\&=1-2\sum_{n=1}^{\infty}\frac{J_0(r\,r_n)}{r_n J_1(r_n)}E_{\alpha}\left(-\frac{b_2 r_n^2}{Pr}t^{\alpha}\right).\end{aligned} \tag{3.7}$$

The mathematical formula for Nusselt number is given by [11]

$$NU=-\left(\frac{\partial\theta(r,t)}{\partial r}\right)\Big|_{r=1}=2\sum_{n=1}^{\infty}E_{\alpha}\left(-\frac{b_2 r_n^2}{Pr}t^{\alpha}\right). \tag{3.8}$$

Figure 1a illustrates that with increasing time, the temperature profile increases. Due to fractional approach, the point temperature is influenced by the historical temperature profile, leading to potentially faster changes with increasing the fractional order α and the radius r as shown in Fig.1b.

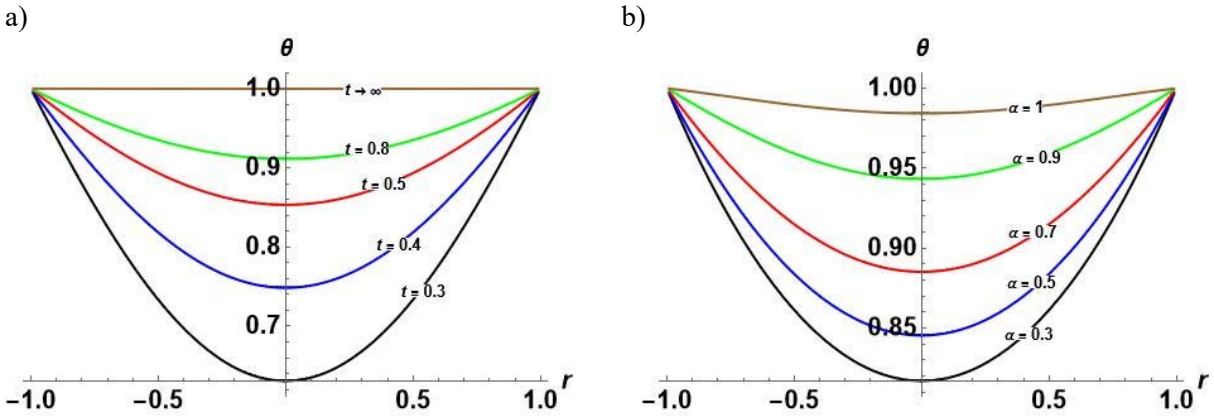

Fig.1. Plot of the $\theta(r,t)$ Eq.(3.7): a) when $\alpha=0.8,\ Pr=1,\ b_2=1$ at various values of t, b) when $Pr=b_2=1,\ t=0.8$ at different values of α.

c)

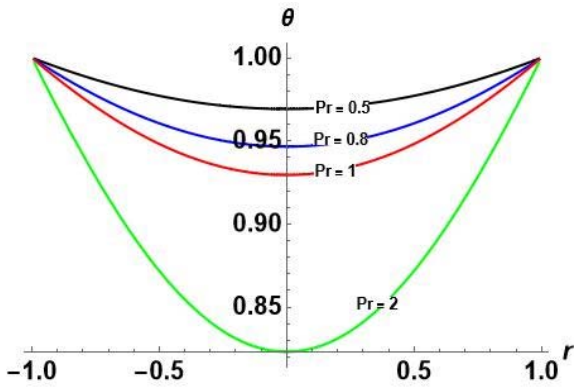

Fig.1 cont. Plot of the $\theta(r,t)$ Eq.(3.7): c) when $t = b_2 = 1,\ \alpha = 0.8$ at various values of Pr.

Figure 1c shows that with increasing the Prandtl number Pr the temperature profile decreases as the high Prandtl number fluids lead to a thin thermal boundary layer and a sharp temperature gradient.

a)

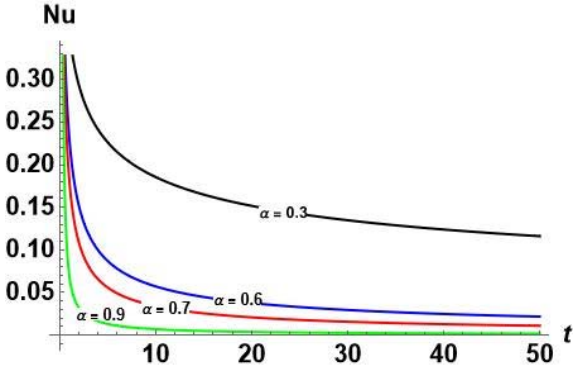

b)

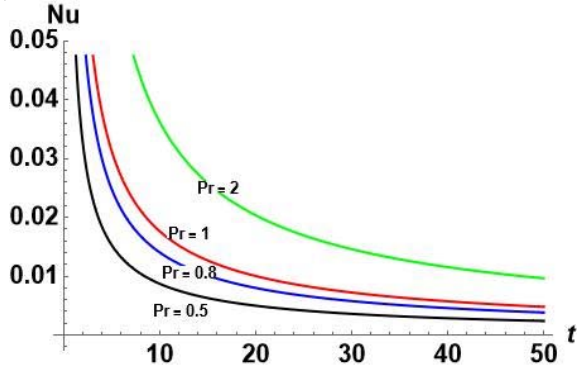

Fig.2. Plot of the NU Eq.(3.8): a) when $b_2 = 1, Pr = 1$ at various values of α,
b) when $b_2 = 1, \alpha = 0.8$ at various values of Pr.

Figure 2a illustrates that with decreasing α the Nusselt number increases as the lower α values often correspond to less complex diffusion behavior and more effective convective heat transfer, approaching classical heat transfer scenarios where the Nusselt number is higher. During the initial stages of heat transfer, the temperature gradients are steep, leading to a higher Nusselt number. And as the system reaches thermal equilibrium, the Nusselt number may decrease as the temperature gradients diminish. Also the Prandtl number affects how quickly the system reaches thermal equilibrium, thus indirectly influencing the time-dependent behavior of the Nusselt number as obtained in Fig.2b.

4. Exact solution for the velocity of the fluid

Applying the FHT (2.4) to Eq.(1.7) and utilizing Eq.(2.7), we obtain

$$\begin{aligned} & b_0\, {}_0^c D_t^{\gamma} u(r_n,t) + b_0 \lambda\, {}_0^c D_t^{\beta} u(r_n,t) = \\ & = -r_n^2\, u(r_n,t) + r_n J_1(r_n) u(1,t) + b_1 Gr\, \theta(r_n,t) + b_1 Gr \lambda\, {}_0^c D_t^{\alpha} \theta(r_n,t). \end{aligned} \tag{4.1}$$

Using the condition $u(1,t)=H(t)exp(i\omega t)$, we obtain

$$\begin{aligned} &b_0\,{}_0^cD_t^{\gamma}u(r_n,t)+b_0\lambda\,{}_0^cD_t^{\beta}u(r_n,t)= \\ &=-r_n^2u(r_n,t)+r_nJ_1(r_n)H(t)exp(i\omega t)+b_1Gr\,\theta(r_n,t)+b_1Gr\lambda\,{}_0^cD_t^{\alpha}\theta(r_n,t). \end{aligned} \tag{4.2}$$

Apply the LT to Eq.(4.2), to get

$$\begin{aligned} &b_0\left(s^{\gamma}L\left[u(r_n,t)\right]-s^{\gamma-1}u(r_n,0)\right)+b_0\lambda\left(s^{\beta}L\left[u(r_n,t)\right]-s^{\beta-1}u(r_n,0)-s^{\beta-2}u_t(r_n,0)\right)= \\ &=-r_n^2L\left[u(r_n,t)\right]+r_nJ_1(r_n)\frac{1}{s-i\omega}+b_1Gr\,L\left[\theta(r_n,t)\right]+ \\ &+b_1Gr\lambda\left(s^{\alpha}L\left[\theta(r_n,t)\right]-s^{\alpha-1}\theta(r_n,0)\right). \end{aligned} \tag{4.3}$$

Since $\theta(r_n,0)=0,u(r_n,0)=0,u_t(r_n,0)=0$, we get

$$\begin{aligned} &b_0\left(s^{\gamma}L\left[u(r_n,t)\right]\right)+b_0\lambda\left(s^{\beta}L\left[u(r_n,t)\right]\right)= \\ &=-r_n^2L\left[u(r_n,t)\right]+r_nJ_1(r_n)\frac{1}{s-i\omega}+b_1Gr\,L\left[\theta(r_n,t)\right]+b_1Gr\lambda\left(s^{\alpha}L\left[\theta(r_n,t)\right]\right). \end{aligned} \tag{4.4}$$

Solving Eq.(4.4) for $L\left[u(r_n,t)\right]$ and utilizing Eq.(3.5), we get

$$\begin{aligned} L\left[u(r_n,t)\right]&=\frac{1}{\left(\frac{b_0\lambda}{r_n^2}s^{\beta}+\frac{b_0}{r_n^2}s^{\gamma}+1\right)} \\ &\left(\frac{1}{s-i\omega}\frac{J_1(r_n)}{r_n}+\frac{\frac{b_2r_n^2}{Pr}}{s\left(s^{\alpha}+\frac{b_2r_n^2}{Pr}\right)}\frac{b_1Gr\,J_1(r_n)}{r_n^{\,3}}+\frac{1}{s^{1-\alpha}\left(s^{\alpha}+\frac{b_2r_n^2}{Pr}\right)}\frac{b_1b_2\lambda Gr\,J_1(r_n)}{r_n\,Pr}\right). \end{aligned} \tag{4.5}$$

The application of the inverse LT to Eq.(4.5), in conjunction with Lemma 3, yields

$$\begin{aligned} u(r_n,t)=\int_0^t\sum_{k=0}^{\infty}&\frac{\left(\frac{-b_0}{r_n^2}\right)^k}{\left(\frac{b_0\lambda}{r_n^2}\right)^{k+1}}\tau^{(1+k)\beta-k\gamma-1}E_{\beta,(1+k)\beta-k\gamma}^{k+1}\left(\frac{-r_n^2}{b_0\lambda}\tau^{\beta}\right)\left[\frac{J_1(r_n)}{r_n}e^{i\omega(t-\tau)}+\right. \\ &\left.+\frac{b_1Gr\,J_1(r_n)}{r_n^{\,3}}\left(1-E_{\alpha}\left(-\frac{b_2r_n^2}{Pr}(t-\tau)^{\alpha}\right)\right)+\frac{b_1b_2\lambda GrJ_1(r_n)}{r_n\,Pr}\left(E_{\alpha}\left(-\frac{b_2r_n^2}{Pr}(t-\tau)^{\alpha}\right)\right)\right]dt. \end{aligned} \tag{4.6}$$

Utilizing Lemma 4, we get

$$u(r_n,t)=\sum_{k=0}^{\infty}\sum_{p=0}^{\infty}(-1)^{k+p}\left(\frac{r_n^2}{b_0\lambda}\right)^{p+1}\frac{(k+1)_p}{(p)!}\left(\frac{1}{\lambda}\right)^k t^{(k+p+1)\beta-k\gamma}\frac{J_1(r_n)}{r_n}$$
$$\left[E_{1,1+(k+p+1)\beta-k\gamma}(i\omega t)+\frac{b_1 Gr}{r_n^2}\frac{1}{\Gamma((k+p+1)\beta-k\gamma+1)}+\right. \tag{4.7}$$
$$\left.+\left(\frac{b_1 b_2\lambda Gr}{Pr}-\frac{b_1 Gr}{r_n^2}\right)E_{\alpha,1+(k+p+1)\beta-k\gamma}\left(-\frac{b_2 r_n^2}{Pr}t^{\alpha}\right)\right].$$

By applying inverse FHT Eq.(2.5) to Eq.(37), we obtain

$$u(r,t)=2\sum_{n=1}^{\infty}\sum_{k=0}^{\infty}\sum_{p=0}^{\infty}(-1)^{k+p}\frac{J_0(r r_n)}{r_n\ J_1(r_n)}\left(\frac{r_n^2}{b_0\lambda}\right)^{p+1}\frac{(k+1)_p}{(p)!}\left(\frac{1}{\lambda}\right)^k t^{(k+p+1)\beta-k\gamma}$$
$$\left[E_{1,1+(k+p+1)\beta-k\gamma}(i\omega t)+\frac{b_1 Gr}{r_n^2}\frac{1}{\Gamma((k+p+1)\beta-k\gamma+1)}+\right. \tag{4.8}$$
$$\left.+\left(\frac{b_1 b_2\lambda Gr\, r_n^2-b_1 Gr\, Pr}{r_n^2\, Pr}\right)E_{\alpha,1+(k+p+1)\beta-k\gamma}\left(-\frac{b_2 r_n^2}{Pr}t^{\alpha}\right)\right].$$

For $\lambda=0$, the solution $u(r,t)$ is

$$u(r,t)=2\sum_{n=1}^{\infty}\frac{r_n\ J_0(r r_n)}{b_0\ J_1(r_n)}\left[\frac{b_1 b_2 Gr}{Pr}t^{\gamma}E_{\gamma,\gamma+1}\left(-\frac{r_n^2}{b_0}t^{\gamma}\right)+\sum_{p=0}^{\infty}\left(\frac{-r_n^2}{b_0}\right)^p t^{\gamma p+\gamma}E_{1,\gamma p+\gamma+1}(i\omega t)+\right.$$
$$\left.-\frac{b_1 b_2 Gr}{Pr}\sum_{p=0}^{\infty}\left(\frac{-r_n^2}{b_0}\right)^p t^{\gamma p+\gamma}E_{\alpha,\gamma p+\gamma+1}\left(-\frac{b_2 r_n^2}{Pr}t^{\alpha}\right)\right]. \tag{4.9}$$

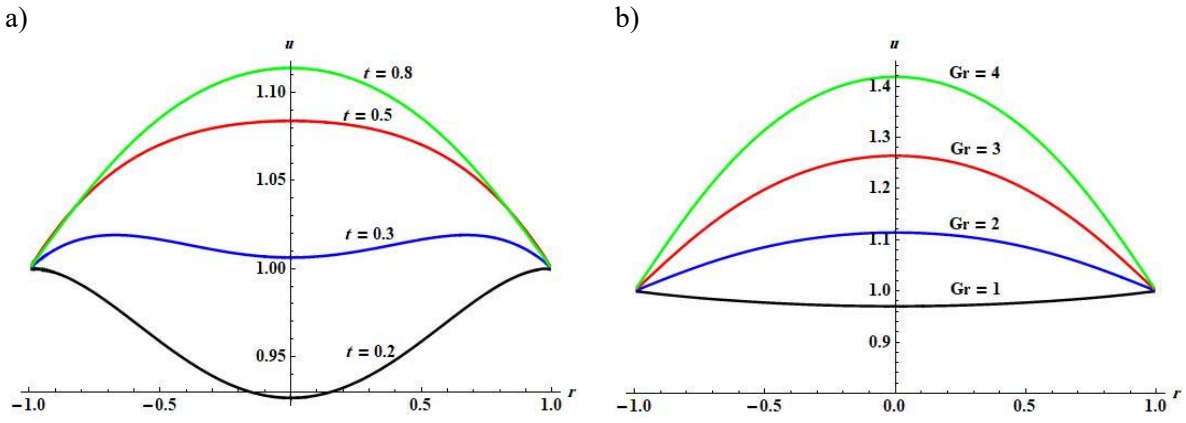

Fig.3. Plot of the velocity profile Eq.(4.9) when $b_0=b_1=b_2=\omega=1$, and:
a) $Pr=Gr=2,\alpha=\gamma=0.5$ at different times,
b) $Pr=2,t=0.8$ and $\alpha=\gamma=0.5$ at various values of Gr.

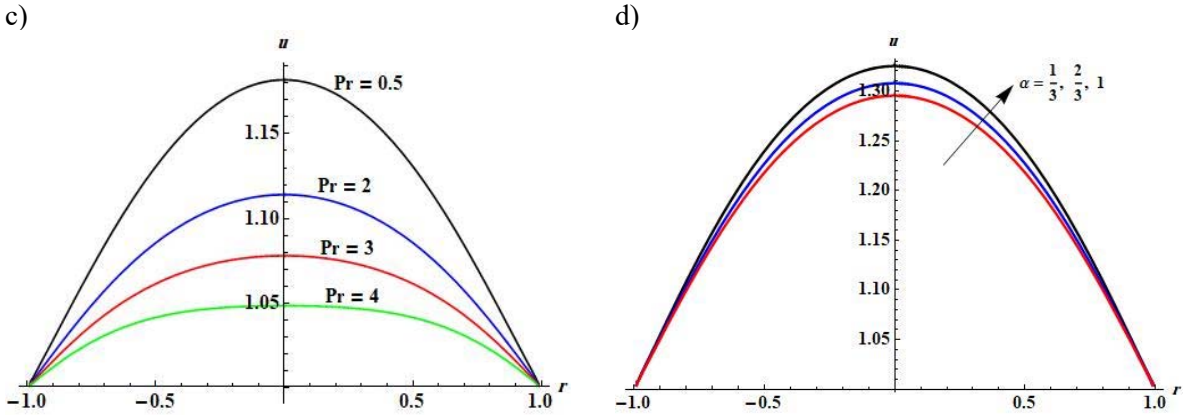

Fig.3 cont. Plot of the velocity profile Eq.(4.9) when $b_0 = b_1 = b_2 = \omega = 1$, and:
c) $Gr = 2$, $t = 0.8$ and $\alpha = \gamma = 0.5$ at various values of Pr,
d) $Pr = Gr = 2$, $t = 0.8$ and $\gamma = 1$ at various values of α.

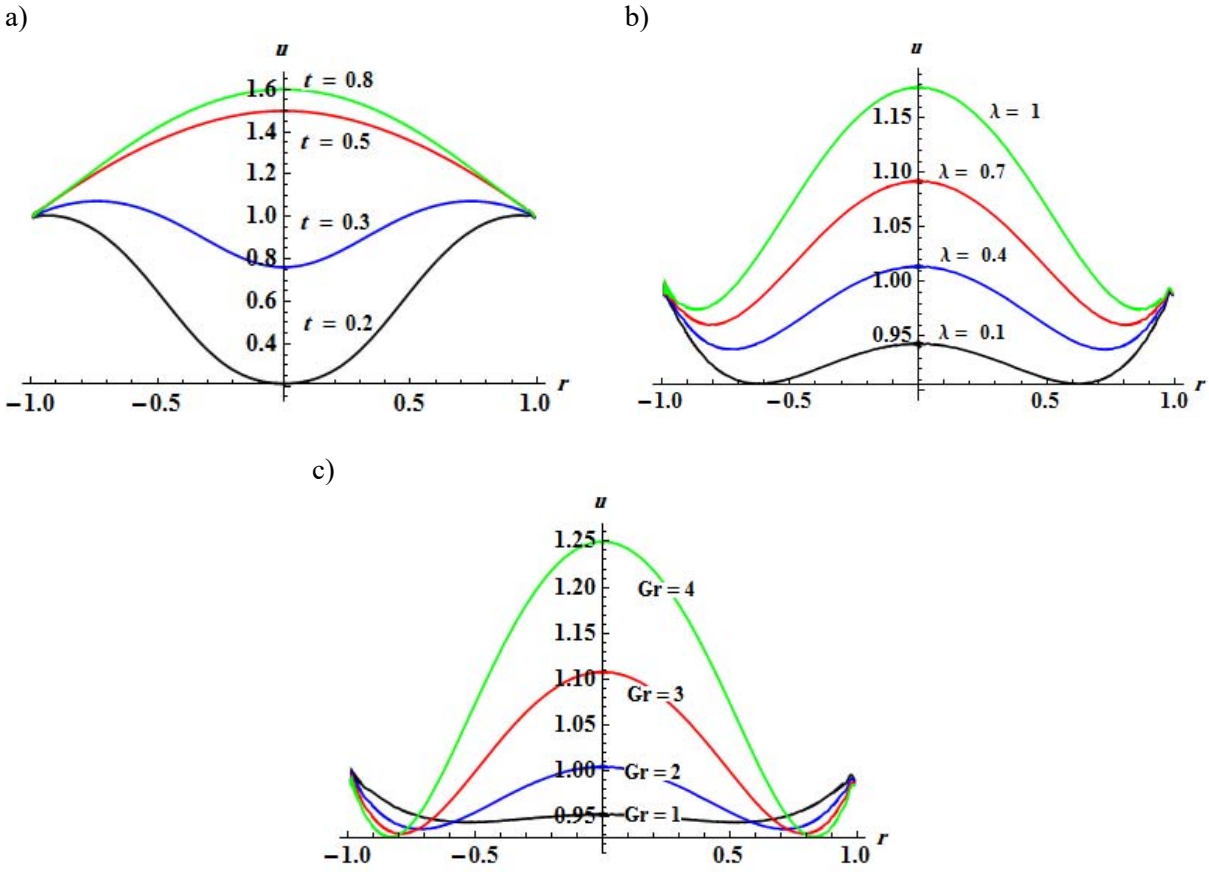

Fig.4. Plot of the velocity profile Eq.(4.8) when $b_0 = b_1 = b_2 = 1$, and:
a) $Pr = 1$, $Gr = 2$, $\omega = 1$, $\alpha = \gamma = 0.75$, $\beta = 1.5$, $\lambda = 0.6$ at various of times,
b) $Pr = 1$, $Gr = 2$, $\omega = 1$, $\alpha = \gamma = 0.75$, $\beta = 1.5$, $t = 2$ at various values of λ,
c) $Pr = 2$, $\omega = 1$, $\alpha = \gamma = 0.75$, $\beta = 1.5$, $\lambda = 0.4$ and $t = 2$ at various values of Gr.

For $\lambda = 0$, we can see that: the velocity profile increases with increasing the time t (see Fig.3a). An increase in Gr corresponds to a rise in the velocity profile (see Fig.3b) due to the growing of the relative influence of buoyancy forces. With decreasing Pr, the velocity profile increases (see Fig.3c) as lowering Prandtl number means that thermal diffusivity is higher relative to momentum diffusivity. Figure 3d demonstrates that the velocity profile rises in conjunction with an increase in α.

For $\lambda \neq 0$ we can notice that: the velocity profile increases with increasing the time t (see Fig.4a) more than that happened before in Fig.3a. Figure 4b illustrates that with increasing the Maxwell fluid parameter λ the velocity profiles increase due to the increasing in elastic response and longer relaxation time. Also, the velocity profile increases with increasing Gr, but the velocity profile decreases when $|r|$ approaches to *1* due to boundary effects or constraints in the system that limit the fluid's velocity near the edges or boundaries (see Fig.4c).Through our study of the model in fractional form, we obtain results that are more advanced than those obtained previously, and through comparison with non-fractal alpha values in certain cases, we were able to obtain the same values previously observed in [11].

5. Conclusions

To obtain the exact solutions for the fractional systems Eq.(1.6) and Eq.(1.7) under the boundary conditions specified in Eq.(1.3), Laplace and finite Hankel transforms are applied. The derived formulas for the temperature profile, Nusselt number, and velocity profile allow for the determination of all interrelations among the factors in both the absence and presence of MoS_2 + GO hybrid nanocomposites.

Nomenclature

b_0, b_1, b_2 – coefficients
$E_\alpha(z)$ – ML function
$E_{\alpha,\beta}(z)$ – the two parameters ML function
$E^{\gamma}_{\alpha,\beta}(z)$ – the three parameters ML function
FHT – finite Hankel transform
Gr – Grashof number
$H(t)$ – unit step function
LT – Laplace transform
OVC – oscillating vertical cylinder
Pr – fluid Prandtl number
r – radial coordinate
T – time
u – fluid velocity
θ – fluid temperature
λ – Maxwell fluid parameter
ω – oscillation frequency

References

[1] Yunus A.C. (2003): *Heat Transfer: a Practical Approach*.– MacGraw Hill, New York, p.210.

[2] Fetecau C., Mahmood A., Fetecau C. and Vieru D., (2008): *Some exact solutions for the helical flow of a generalized Oldroyd-B fluid in a circular cylinder*.– Computers & Mathematics with Applications, vol.56, No.12, pp.3096-3108.

[3] Mozafarifard M. and Toghraie D. (2020): *Numerical analysis of time-fractional non-Fourier heat conduction in porous media based on Caputo fractional derivative under short heating pulses*.– Heat and Mass Transfer, vol.56, No.11, pp.3035-3045.

[4] El-Kalla I. (2011): *Error estimate of the series solution to a class of nonlinear fractional differential equations*.– Communications in Nonlinear Science and Numerical Simulation, vol.16, No.3, pp.1408-1413.

[5] Musurmanov R.K., Utaev S.A. and Kasimov I.S. (2021): *Mathematical modeling of changes in the physical and chemical properties of gas engine oils*.– In IOP Conference Series: Earth and Environmental Science, vol.868, No.1, p.012044.

[6] Mousazade M.R., Sedighi M., Manesh M.H.K. and Ghasemi, M. (2022): *Mathematical modeling of waste engine oil gasification for synthesis gas production; operating parameters and simulation*.– International Journal of Thermodynamics, vol.25, No.1, pp.65-77.

[7] Kumbár V., and Sabaliauskas A. (2013): *Low-temperature behaviour of the engine oil*.– Acta Universitatis Agriculturae et Silviculturae Mendelianae Brunensis, vol.61, No.6, pp.1763-1767.

[8] Khan I., Ali Shah N., Tassaddiq A., Mustapha N. and Kechil S.A. (2018): *Natural convection heat transfer in an oscillating vertical cylinder*.– PloS one, vol.13, No.1, p.e0188656.

[9] Arif M., Kumam P., Khan D. and Watthayu W. (2021): *Thermal performance of GO-MoS2/engine oil as Maxwell hybrid nanofluid flow with heat transfer in oscillating vertical cylinder*.– Case Studies in Thermal Engineering, vol.27, p.101290.

[10] Sobhani H., Azimi A., Noghrehabadi A. and Mozafarifard M. (2023): *Numerical study and parameters estimation of anomalous diffusion process in porous media based on variable-order time fractional dual-phase-lag model*.– Numerical Heat Transfer, Part A: Applications, vol.83, No.7, pp.679-710.

[11] Zhao J., Zheng L., Zhang X. and Liu F. (2016): *Unsteady natural convection boundary layer heat transfer of fractional Maxwell viscoelastic fluid over a vertical plate*.– International Journal of Heat and Mass Transfer, vol.97, pp.760-766.

[12] Raza A., Al-Khaled K., Khan M.I., Khan S.U., Farid S., Haq A.U. and Muhammad T. (2021): *Natural convection flow of radiative Maxwell fluid with Newtonian heating and slip effects: Fractional derivatives simulations*.– Case Studies in Thermal Engineering, vol.28, p.101501.

[13] Chang T., Li Y., Jiang Y., Li S., Chen X. and Ji Y. (2023): *Study on unsteady natural convection heat transfer of crude oil storage tank based on fractional-order Maxwell model*.– Physics of Fluids, vol.35, No.11, https://doi.org/10.1063/5.0172017.

[14] Sehra S., Noor A., Haq S.U., Jan S.U., Khan I. and Mohamed A. (2023): *Heat transfer of generalized second grade fluid with MHD, radiation and exponential heating using Caputo-Fabrizio fractional derivatives approach*.– Scientific Reports, vol.13, No.1, p.5220.

[15] Sehra Sadia H., Haq S.U., Alhazmi H., Khan I. and Niazai, S. (2024): *A comparative analysis of three distinct fractional derivatives for a second grade fluid with heat generation and chemical reaction*.– Scientific Reports, vol.14, No.1, p.4482.

[16] Sadia H., Haq S.U., Khan I., Ashmaig M.A.M. and Omer A.S. (2023): *Time fractional analysis of generalized Casson fluid flow by YAC operator with the effects of slip wall and chemical reaction in a porous medium*.– International Journal of Thermofluids, vol.20, p.100466.

[17] Jan S.U., Haq S.U., Ullah N., Ullah W., Sehra and Khan I. (2023): *Heat transfer analysis of generalized second-grade fluid with exponential heating and thermal heat flux*. Scientific Reports, vol.13, No.1, p.16934.

[18] Khan S., Sadia H., Haq S.U. and Khan I. (2023): *Time fractional Yang–Abdel–Cattani derivative in generalized MHD Casson fluid flow with heat source and chemical reaction*.– Scientific Reports, vol.13, No.1, p.16494.

[19] Khan S., Iftikhar W., Haq S.U., Jan S.U., Khan, I. and Mohamed, A. (2022): *Caputo–Fabrizio fractional model of MHD second grade fluid with Newtonian heating and heat generation*.– Scientific Reports, vol.12, No.1, p.22371.

[20] Mathai A.M. and Haubold H.J. (2017): *An Introduction to Fractional Calculus Book*.– Hauppauge, New York, Nova Science Publishers.

[21] Debnath L. and Bhatta D. (2016): *Integral Transforms and Their Applications*.– Chapman and Hall/CRC.

[22] Neuman E. (2013): *Inequalities and bounds for the incomplete gamma function*.– Results in Mathematics, vol.63, pp.1209-1214.

[23] Chaudhry M.A. and Zubair S.M. (2002): *Extended incomplete gamma functions with applications*.– Journal of mathematical analysis and applications, vol.274, No.2, pp.725-745.

[24] Sandev T. and Tomovski Ž. (2019): *Fractional Equations and Models: Theory and Applications*.– Developments in Mathematics, Springer Cham, p.345.

Received: February 24, 2025
Revised: October 16, 2025